ACS APPLIED MATERIALS & INTERFACES

Research Article

www.acsami.org

# Interfacial Electron-Shuttling Processes across KolliphorEL Monolayer Grafted Electrodes

Khadijeh Nekoueian,[†,‡,§] Christopher E. Hotchen,[†] Mandana Amiri,[‡] Mika Sillanpää,[§] Geoffrey W. Nelson,[∥] John S. Foord,[⊥] Philip Holdway,[#] Antoine Buchard,[†] Stephen C. Parker,[†] and Frank Marken*[,†]

[†]Department of Chemistry, University of Bath, Bath BA2 7AY, United Kingdom

[‡]Department of Chemistry, University of Mohaghegh Ardabili, Ardabil 56199-11367, Iran

[§]Laboratory of Green Chemistry, School of Engineering Science, Lappeenranta University of Technology, Sammonkatu 12, FI-50130 Mikkeli, Finland

[∥]Imperial College London, Department of Materials, Royal School of Mines, Exhibition Road, London SW7 2AZ, United Kingdom

[⊥]Chemistry Research Laboratories, Oxford University, South Parks Road, Oxford OX1 3TA, United Kingdom

[#]Department of Materials, Oxford University, Begbroke Science Park, Begbroke Hill, Oxford OX5 1PF, United Kingdom

**ABSTRACT:** Covalently grafted KolliphorEL (a poly(ethylene glycol)-based transporter molecule for hydrophobic water-insoluble drugs; MW, ca. 2486; diameter, ca. 3 nm) at the surface of a glassy-carbon electrode strongly affects the rate of electron transfer for aqueous redox systems such as $Fe(CN)_6^{3-/4-}$. XPS data confirm monolayer grafting after electrochemical anodization in pure KolliphorEL. On the basis of voltammetry and impedance measurements, the charge transfer process for the $Fe(CN)_6^{3-/4-}$ probe molecule is completely blocked after KolliphorEL grafting and in the absence of a "guest". However, in the presence of low concentrations of suitable ferrocene derivatives as guests, mediated electron transfer across the monolayer via a shuttle mechanism is observed. The resulting amplification of the ferrocene electroanalytical signal is investigated systematically and compared for five ferrocene derivatives. The low-concentration electron shuttle efficiency decreases in the following sequence: (dimethylaminomethyl)ferrocene > *n*-butyl ferrocene > ferrocene dimethanol > ferroceneacetonitrile > ferroceneacetic acid.

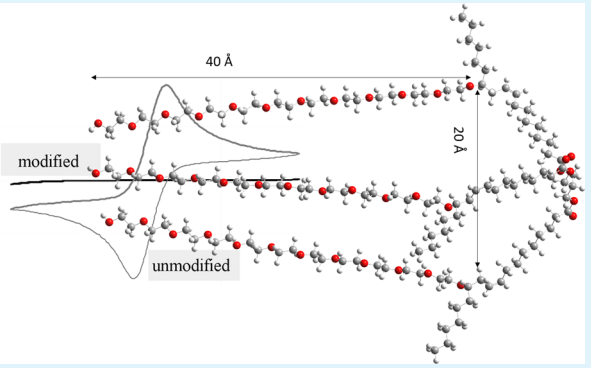


**KEYWORDS:** *Cremophor, PEGylation, amplification, voltammetry, tunneling, sensor*

## 1. INTRODUCTION

Surface-modified electrodes are widely used in sensors[1] and in film electrodes.[2−4] Covalent grafting of a monolayer onto carbon electrode surfaces can be achieved by diazonium methods,[5,6] "click" chemistry,[7] amide chemical attachment,[8] or many other similar processes.[9] Electrochemical surface modification offers the advantage (over chemical processes) of potential control and optimization to achieve well-defined monolayer coverage. A wide range of often radical-based intermediates are known to attach spontaneously to carbon electrode surfaces.[10,11] We have recently adapted a methodology introduced by Maeda and co-workers[12,13] to attach poly(ethylene glycol) (PEG) derivatives to glassy-carbon and boron-doped diamond electrode surfaces.[14] An anodic treatment was developed to allow monolayer attachment of PEGs with a resulting structure-dependent retardation of the rate of heterogeneous electron transfer. In this study, a PEGylated castor oil derivative, KolliphorEL (CAS no. 61791-12-6; MW, ca. 2486 g $mol^{-1}$; Figure 1) is selected to demonstrate this anodic grafting process for a more complex molecule.

For PEGylated molecules such as KolliphorEL, the hydroxyl end groups are sensitive to oxidation with radical intermediates likely to bind to the carbon electrode surface.[15] As a PEGylated castor oil derivative, KolliphorEL (Figure 1) is often employed as medicinal additive or drug carrier reagent[16] to allow water-insoluble drug molecules to be solubilized and carried to the location of action. On the basis of this use, it could introduce interesting new properties (with a hydrophobic layer, Figure 1C) to the modified carbon electrode surface. Similarly, PEGylation is widely used to impose hydrophilic character to surfaces, particles, and molecules.[17] In this study, the KolliphorEL surface layer is employed as (i) a barrier to electron transfer and (ii) a host film to allow hydrophobic

Received: April 27, 2015
Accepted: June 24, 2015
Published: June 24, 2015





DOI: 10.1021/acsami.5b03654
ACS Appl. Mater. Interfaces 2015, 7, 15458−15465

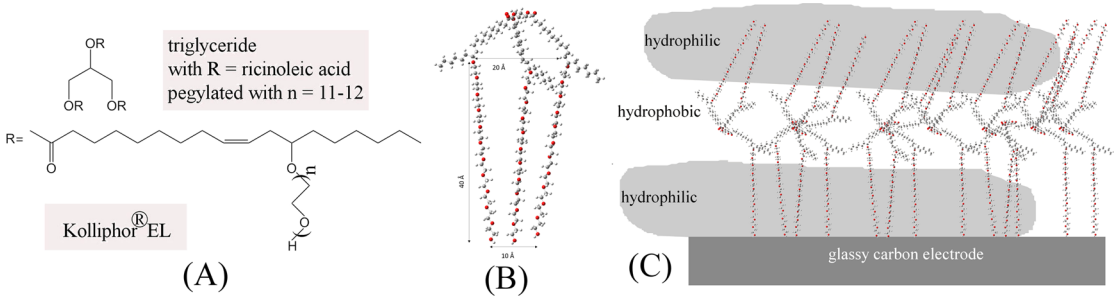


**Figure 1.** (A) Molecular structure of the main component in KolliphorEL and (B) 3D rendering (GaussView 5.0) showing the approximate diameter of 3−5 nm. (C) Schematic drawing of a KolliphorEL monolayer with a hydrophobic region resulting from the triglyceride.

reagents to bind and enhance or amplify interfacial electron transfer.

Amplification of electroanalytical signals is often desirable and possible, for example, (i) by direct feedback in generator-collector electrode devices[18] and (ii) in catalytic processes where an enzyme[19] or nanoparticle catalyst[20] is employed to enhance the analytical response. Here, amplification is achieved simply on the basis of a difference in the rate of heterogeneous electron transfer for two redox systems. Figure 2 shows a schematic drawing of the electrode surface with a layer of KolliphorEL immobilized. The direct electron transfer to the $Fe(CN)_6^{3-/4-}$ redox system is suppressed, but the presence of a shuttle molecule such as ferrocene (Fc) can be employed to restore electron transfer. Very low concentrations of ferrocene can therefore be detected as relatively large amplified currents.

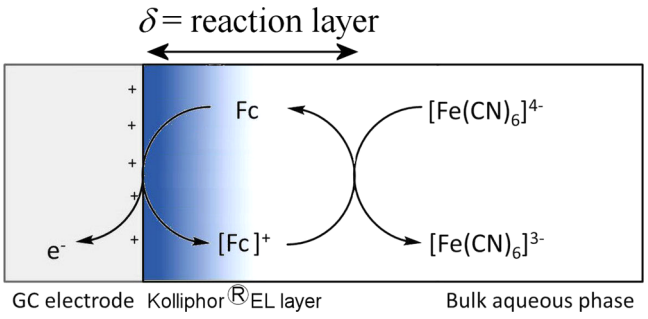


**Figure 2.** Schematic drawing of the amplification mechanism for the low-concentration ferrocene (Fc) redox process in the presence of the suppressed $Fe(CN)_6^{3-/4-}$ electron transfer.

Here, the Maeda method is employed to produce a KolliphorEL monolayer on a glassy-carbon electrode surface. It is shown that this results in a dramatic decrease in the rate of heterogeneous electron transfer for aqueous $Fe(CN)_6^{3-/4-}$. Ferrocene derivatives are then compared with respect to their shuttle ability for electrons to pass through the KolliphorEL layer. A quantitative study reveals the structural parameters that govern the shuttle process. Future applications are envisaged in the amplification (or modulation) of other types of electron-transfer processes, e.g., in analytical drug or explosives detection applications.

## 2. EXPERIMENTAL SECTION

**2.1. Chemical Reagents.** KolliphorEL (CAS number 61791-12-6; MW ca. 2450 g $mol^{-1}$; previously also known as Cremophor EL; Aldrich) is a PEGylated castor oil derivative (Figure 1). Lithium perchlorate ($LiClO_4$, Sigma-Aldrich, ≥ 95%, ACS reagent grade) was used as background electrolyte in neat KolliphorEL solutions. Ferrocene dimethanol ($Fc(MeOH)_2$, Aldrich, 98%), ferroceneacetic acid (FcAcOH, Aldrich, 98%), ferroceneacetonitrile (FcMeCN, Aldrich), *n*-butyl ferrocene (BuFc, Alfa Aesar, 98%, oil), *N*,*N*′-(dimethylaminomethyl)ferrocene ($MeFcNMe_2$, TCI Europe, oil), potassium ferrocyanide(II) ($K_4Fe(CN)_6$, Fisons, 98%), and potassium ferricyanide(III) ($K_3Fe(CN)_6$, Aldrich, 99+ %) were used as redox species in aqueous solutions containing 0.1 M potassium nitrate ($KNO_3$, Sigma-Aldrich, ≥ 99.0%) as background electrolyte.

**2.2. Instrumentation.** All electrochemical measurements were carried out using an Ivium Compactstat 104 Model B08084 (Ivium Technologies NL). A step potential of 1 mV was used in cyclic voltammetry experiments. Electrochemical impedance spectroscopy (EIS) was carried out at open-circuit potential (OCP) = 0.19 V versus SCE in a 0.1 M $KNO_3$ solution containing 5 mM $Fe(CN)_6^{3-}$ and 5 mM $Fe(CN)_6^{4-}$, with an amplitude of 10 mV. The frequency was varied from 10 kHz to 0.01 Hz. Equivalent circuit data fitting was carried out using ZView software.

X-ray photoelectron spectroscopy (XPS) experiments were carried out using a Thermo K Alpha (Thermo Scientific) spectrometer (operating at ~$10^{-8}$−$10^{-9}$ Torr), a 180° double-focusing hemispherical analyzer running in constant-analyzer energy (CAE) mode with a 128-channel detector. A monochromated Al K$\alpha$ radiation source (1486.7 eV) was used. Peak fitting was carried out with XPS Peak Fit (v. 4.1) software using Shirley background subtraction. Peaks were referenced to the adventitious carbon C 1s peak (284.6 eV), and peak areas were normalized to the photoelectron cross section of the F 1s photoelectron signal using atomic sensitivity factors.[21]

**2.3. Procedure for KolliphorEL Grafting.** KolliphorEL is a viscous liquid and can be employed directly as a solvent in electrochemical experiments after addition of suitable electrolyte. Here, a solution of 20 mM $LiClO_4$ in KolliphorEL is employed for the electrode modification process. A 3 mm diameter glassy-carbon electrode is placed into this solution with +1.6 V versus SCE applied for 20 min (optimized previously).[14] The electrode is then rinsed with water and dried. The extent of surface modification is apparent from XPS data for two independently prepared samples K1 and K2 (Figure 3).

Survey spectra show photoelectron signals from contaminant-free surfaces containing C and O (Figure 3A). The C 1s photoelectron signals show evidence for a PEG-like interface. The C 1s spectra associated with KolliphorEL samples K1 and K2 are shown in Figure 3B. The spectra could be fitted (section 2) into four chemical environments: adventitious carbon and hydrocarbon (284.6 eV), ether (C−O, ~286.1 eV), carbonyl (C═O, ~287.1 eV), and carboxyl (C═O(OH), ~288.1 eV).[22] The O 1s photoelectron signal in Figure 3C was curve-fitted using the model established by Schlapak et al.[23] as follows: hydroxyl (−OH, ~531 eV), ether (C−O, ~532.2 eV), and water ($H_2O$, ~533.5 eV). The above spectra are consistent with PEG-like surface chemistry, with contribution from C−O from repeated poly(ethylene glycol) units dominating the observed photoelectron signal. The presence of hydroxyl and water O 1s signals suggests that trace water is present within the interface, which is to be expected because water binds strongly to PEG. XPS data are summarized in Table 1. Variation between samples K1 and K2 suggest some position dependence and/or sample-to-sample variability. Key changes in comparison to the bare glassy-carbon surface are (i) an increase in O


DOI: 10.1021/acsami.5b03654
ACS Appl. Mater. Interfaces 2015, 7, 15458−15465

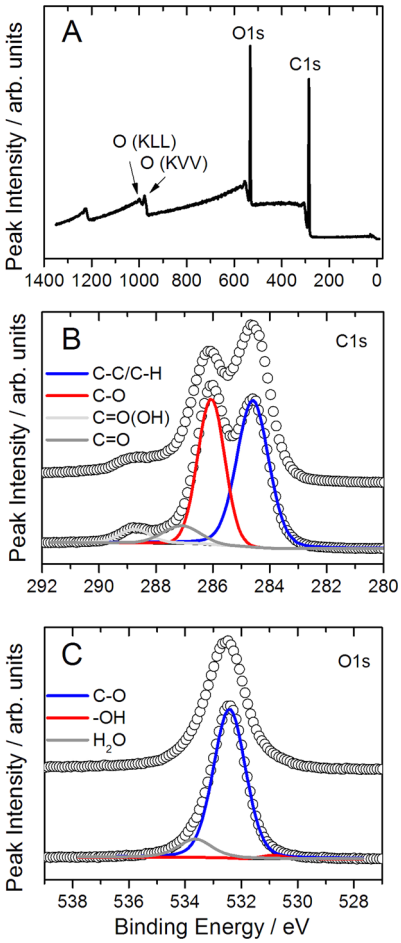


**Figure 3.** (A) Representative survey XPS spectra of KolliphorEL modification of glassy carbon. XPS core level spectra of modified substrate (B) C 1s and (C) O 1s. Representative curve fits (section 2) are shown for C 1s and O 1s and for two independently investigated samples (dotted lines K1, bottom, and K2, above; Table 1).

1s/C 1s ratio, mainly caused by C−O, (ii) an increase in C 1s for C−O, and (iii) an increase in O 1s for C−O.

## 3. RESULTS AND DISCUSSION

**3.1. KolliphorEL Grafting Affects Heterogeneous Electron-Transfer Kinetics.** KolliphorEL is medicinal formulation additive and a transporter molecule for drugs and poorly water-soluble materials.[16] It is employed here when grafted as a monolayer directly onto glassy-carbon electrode surfaces. Although only monolayer deposition occurs, a dramatic effect of this surface modification is detected in heterogeneous electron transfer for the $Fe(CN)_6^{3-/4-}$ redox system (eq 1).

$$Fe(CN)_6^{3-} + e^- \rightleftarrows Fe(CN)_6^{4-} \quad (1)$$

This redox system is often employed to probe surface-modification effects,[24] and here it is shown to be highly sensitive to KolliphorEL grafts. Figure 4A displays cyclic voltammetry data first for the unmodified glassy-carbon electrode and then for the KolliphorEL-modified electrode. The heterogeneous electron transfer to $Fe(CN)_6^{3-/4-}$ is almost completely suppressed within the potential range investigated here. The approximate diameter of the KolliphorEL molecules is 1 nm (Figure 1), which appears to be sufficient to essentially switch off heterogeneous electron transfer. A gentle polish is sufficient to reverse the effect.

The experiment was repeated with impedance analysis to explore the effect in the time domain. Figure 4B shows impedance data for unmodified and modified electrodes. For the unmodified electrode, a conventional Randles circuit model (inset in Figure 4B) was employed giving $R_{sol}$ = 154 Ω, $R_{et}$ = 266 Ω, $C$ = 1.8 μF, $W_P$ = 0.5, $W_T$ = 107, and $W_R$ = 6310 Ω. (The line of best fit overlays data in Figure 4B.) For the KolliphorEL-modified electrode, the impedance response is associated mainly with capacitive charging (Figure 4B), with $R_{sol}$ and $C$ values similar to those for the unmodified electrode. However, a good fit was not possible. This is believed to be due to low-frequency data revealing additional complexity, which could be due to some remaining porosity in the grafted layer and associated with some electron transfer at frequencies below 1 Hz. In summary, the KolliphorEL grafting strongly suppresses electron transfer to $Fe(CN)_6^{3-/4-}$, and it is now possible to introduce guest molecules to explore shuttle effects and changes in electron transfer.

**3.2. KolliphorEL Grafting Affecting Heterogeneous Electron-Transfer Kinetics: Ferrocene Mediators.** In contrast to the dramatic change in the rate of heterogeneous electron transfer observed for hydrophilic $Fe(CN)_6^{3-/4-}$, the rates of electron transfer for many more hydrophobic ferrocene derivatives are potentially less sensitive to surface modification. This is consistent with the less hydrated and more hydrophobic ferrocene derivatives penetrating into the KolliphorEL film and effectively operating as electron shuttles between the electrode surface and the solution redox species (such as $Fe(CN)_6^{3-/4-}$). The shuttle efficiency is investigated for five different ferrocene derivatives.

Ferrocene dimethanol (Figure 5) is modestly water-soluble and employed here as an electron shuttle at 0, 5, 10, and 50 μM concentrations to lower the electron-transfer impedance between the electrode and $Fe(CN)_6^{3-/4-}$. The voltammetric signal at the KolliphorEL-modified glassy carbon increases from no signal to 42 μA peak current (Figure 5A), which is close to the diffusion-limited value for the $Fe(CN)_6^{3-/4-}$ species (compare to Figure 4A). The underlying voltammetric signal for the ferrocene dimethanol itself remains insignificant on this

**Table 1. XPS Ratios and Surface Composition for Two Independently Investigated Samples with KolliphorEL monolayer (K1 and K2) and a Bare Glassy-Carbon (GC) Substrate[a]**

| | | C 1s composition (%) | | | | O 1s composition (%) | | |
|---|---|---|---|---|---|---|---|---|
| sample | O 1s/C 1s | C−C | C−O | C=O | C=O(OH) | OH | $H_2O$ | C−O |
| K1 | 2.94 | 39.1 | 50.2 | 6.4 | 4.3 | 1.3 | 12.6 | 86.1 |
| K2 | 3.12 | 54.7 | 33.8 | 4.8 | 6.7 | 5.3 | 12.8 | 81.9 |
| GC | 1.29 | 66 | 11 | 11 | 8 | 12 | 33 | 55 |

[a]Peak integration methods based on literature models for C 1s[17] and O 1s[18] were employed.



DOI: 10.1021/acsami.5b03654
ACS Appl. Mater. Interfaces 2015, 7, 15458−15465

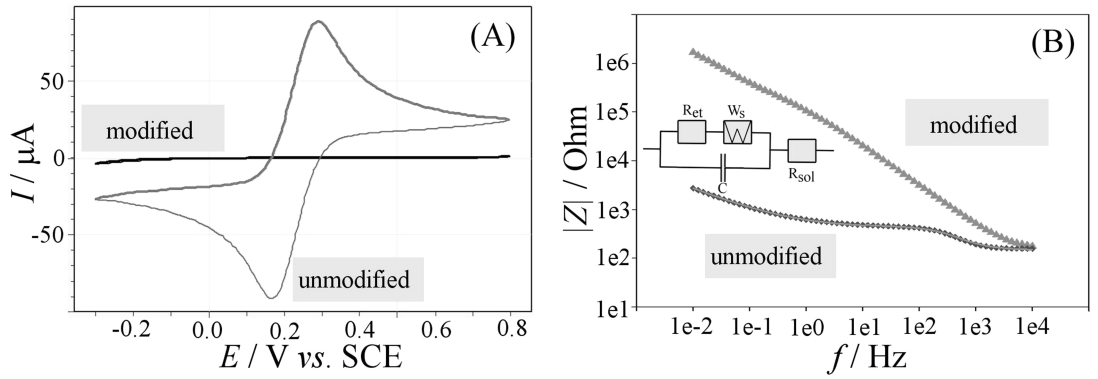


**Figure 4.** (A) Cyclic voltammograms (scan rate = 50 mV $s^{-1}$) for a 3 mm glassy-carbon electrode immersed in aqueous 5 mM $Fe(CN)_6^{3-}$, 5 mM $Fe(CN)_6^{4-}$, and 0.1 M $KNO_3$ before and after KolliphorEL grafting. (B) Impedance data for the same system at the equilibrium potential.

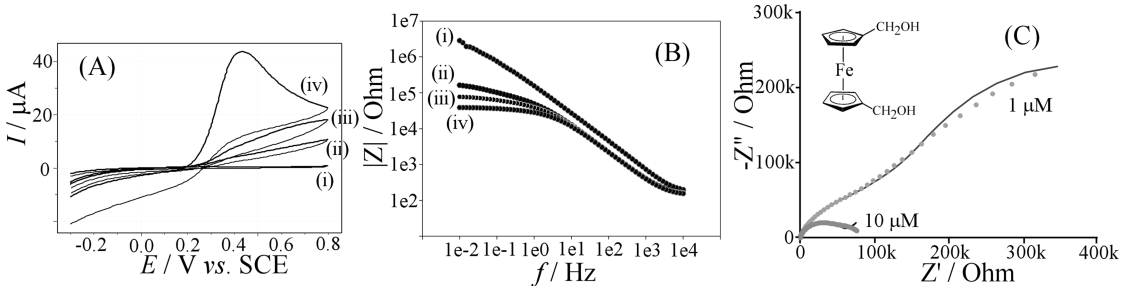


**Figure 5.** (A) Cyclic voltammograms (scan rate = 50 mV $s^{-1}$) for a 3 mm glassy-carbon electrode immersed in aqueous 5 mM $Fe(CN)_6^{3-}$, 5 mM $Fe(CN)_6^{4-}$, and 0.1 M $KNO_3$ with addition of (i) 0, (ii) 5, (iii) 10, and (iv) 50 $\mu$M ferrocene dimethanol. (B) Impedance data for this system at equilibrium potential. (C) Nyquist plot with simulation model data (line) and experimental data (dots) for 1 and 10 $\mu$M ferrocene dimethanol.

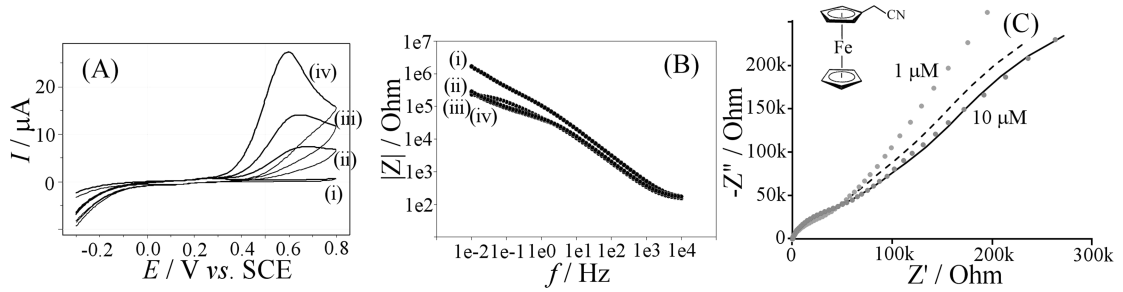


**Figure 6.** (A) Cyclic voltammograms (scan rate = 50 mV $s^{-1}$) for a 3 mm glassy-carbon electrode immersed in aqueous 5 mM $Fe(CN)_6^{3-}$, 5 mM $Fe(CN)_6^{4-}$, and 0.1 M $KNO_3$ with addition of (i) 0, (ii) 5, (iii) 10, and (iv) 50 $\mu$M ferroceneacetonitrile. (B) Impedance data for this system at equilibrium potential. (C) Nyquist plot with simulation model data (dashed and solid lines) and experimental data (dots) for 1 and 10 $\mu$M ferroceneacetonitrile.

scale and is not detected in this experiment. Only the amplified net current for the $Fe(CN)_6^{3-/4-}$ redox system is detected.

The electron shuttle effect is also seen in the impedance data (Figure 5B), where a significant change in the lower-frequency range (below 10 Hz) is consistent with the flow of Faradaic current catalyzed by the ferrocene dimethanol mediator. Figure 5C shows two sets of experimental impedance data (dots) with simulation data (line), which will be discussed below.

When employing ferroceneacetonitrile as the electron shuttle (Figure 6A), a similar change in the cyclic voltammetry peak current is observed. However, the peak currents for oxidation (Figure 6A) appear lower compared to data in Figure 5A, with less cathodic current observed on the reverse scan. Table 2 summarizes some data for voltammetric features (and impedance data, vide infra) observed for the different ferrocene derivatives in experiments at KolliphorEL-modified glassy-carbon electrodes. The reversible potential for $Fe(CN)_6^{4-/3-}$ here is 0.19 V versus SCE, and it can be seen that for all ferrocene derivatives a higher $E_0$ (consistent with less driving force for reduction) makes the amplification process asymmetric with less driving force for the cathodic signal. The magnitude of the anodic peak signal is also likely to be correlated to the peak-to-peak separation $\Delta E_p$ (indicative of slower electron transfer kinetics; Table 2). Therefore, the lower mediated oxidation peaks for ferroceneacetonitrile (Figure 6) and for ferroceneacetic acid (Figure 7), compared to other ferrocene derivatives, are likely to be linked here primarily to the slower kinetics of electron transfer (consistent with a wider peak-to-peak separation) limiting the electron shuttle rate.

Next, ferroceneacetic acid is employed as the electron shuttle (Figure 7), and similar trends are observed. However, the suppression of the oxidation peaks is more pronounced. On the basis of data in Table 2, very similar behavior for ferroceneacetonitrile and ferroceneacetic acid could be predicted, but


DOI: 10.1021/acsami.5b03654
ACS Appl. Mater. Interfaces 2015, 7, 15458−15465

**Table 2. Summary of Data from Voltammetry and Impedance Spectroscopy**[a]

| | $E_0$ (V vs SCE)[b] | $\Delta E_p$ (V)[b] | [Fc] ($\mu$M) | $R_{sol}$ ($\Omega$) | $R_{et}$ ($\Omega$) | $W_R$ (k$\Omega$)[c] | $W_T$ (s)[c] | $CPE_T$ ($\mu$F) | $CPE_P$ | $\delta_{app}$ ($\mu$m) |
|---|---|---|---|---|---|---|---|---|---|---|
| ferrocenedimethanol | 0.28 | 0.11 | 1 | 127 | 9177 | 524 | 38.9 | 2.84 | 0.796 | 153 |
| | | | 10 | 134 | 5073 | 268 | 5.16 | 2.78 | 0.798 | 56 |
| ferroceneacetonitrile | 0.21 | 0.22 | 1 | 137 | 2958 | 690 | 82.5 | 2.39 | 0.816 | 222 |
| | | | 10 | 150 | 5332 | 635 | 67.3 | 2.30 | 0.835 | 201 |
| ferroceneacetic acid | 0.20 | 0.22 | 1 | 123 | 7815 | 1720 | 393 | 2.32 | 0.843 | 486 |
| | | | 10 | 132 | 6063 | 89 | 11.8 | 2.58 | 0.832 | 84 |
| (dimethylaminomethyl)ferrocene | 0.27 | 0.10 | 1 | 135 | 6180 | 123 | 2.82 | 4.01 | 0.795 | 41 |
| | | | 10 | 138 | 3092 | 335 | 19.0 | 2.69 | 0.838 | 107 |
| *n*-butyl ferrocene | 0.22 | 0.04 | 1 | 130 | 6557 | 139 | 8.14 | 1.82 | 0.789 | 70 |
| | | | 10 | 127 | 1117 | 127 | 222 | 3.94 | 0.743 | 365 |

[a]Solution with 50 $\mu$M ferrocene derivative, 5 mM $Fe(CN)_6^{3-}$ and 5 mM $Fe(CN)_6^{4-}$, in 0.1 M $KNO_3$ (scan rate = 50 mV $s^{-1}$). Impedance data relate to a Randles circuit (see text) with $W_P = 0.5$ and $\delta_{app} = (W_T \times D)^{1/2}$, with $D = 0.6 \times 10^{-9}$ $m^2$ $s^{-1}$ as an approximate value[25] used for all ferrocene derivatives. [b]Obtained from cyclic voltammograms of 50 $\mu$M solution of ferrocene derivative in 0.1 M $KNO_3$ at a KolliphorEL-modified glassy-carbon electrode. Note that signals in particular for ferroceneacetonitrile, (dimethylaminomethyl)ferrocene, and *n*-butyl ferrocene are complicated by the interaction with the electrode surface [c]A short Warburg element was selected to reflect the electron transfer to $Fe(CN)_6^{3-/4-}$

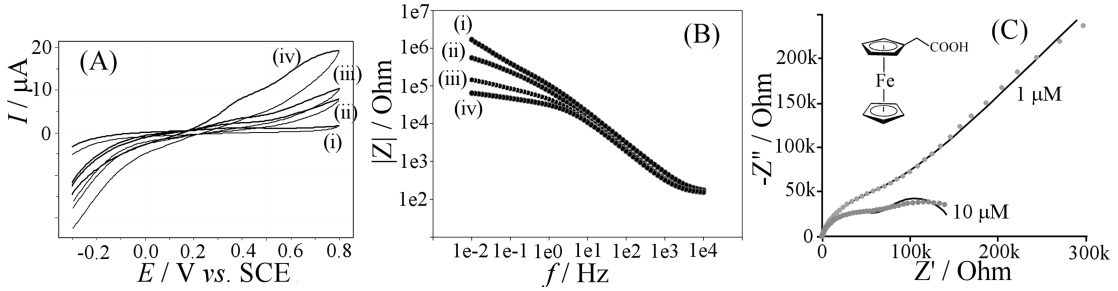


**Figure 7.** (A) Cyclic voltammograms (scan rate = 50 mV $s^{-1}$) for a 3 mm glassy-carbon electrode immersed in aqueous 5 mM $Fe(CN)_6^{3-}$, 5 mM $Fe(CN)_6^{4-}$, and 0.1 M $KNO_3$ with addition of (i) 0, (ii) 5, (iii) 10, and (iv) 50 $\mu$M ferroceneacetic acid. (B) Impedance data for this system at equilibrium potential. (C) Nyquist plot with simulation model data (line) and experimental data (dots) for 1 and 10 $\mu$M ferroceneacetic acid.

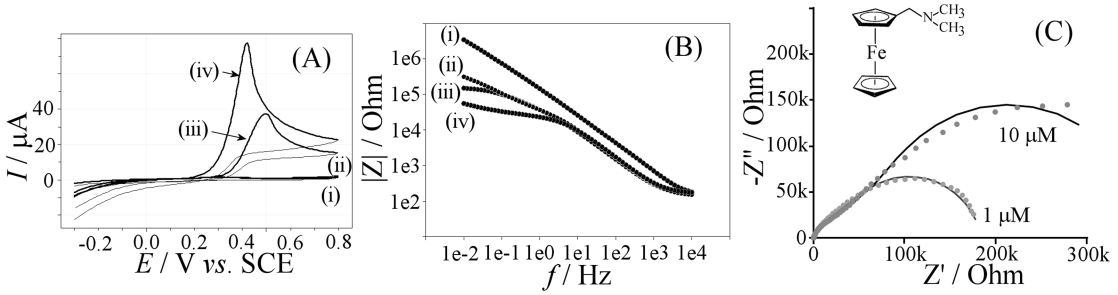


**Figure 8.** (A) Cyclic voltammograms (scan rate = 50 mV $s^{-1}$) for a 3 mm glassy-carbon electrode immersed in aqueous 5 mM $Fe(CN)_6^{3-}$, 5 mM $Fe(CN)_6^{4-}$, and 0.1 M $KNO_3$ with addition of (i) 0, (ii) 5, (iii) 10, and (iv) 50 $\mu$M (dimethylaminomethyl)ferrocene. (B) Impedance data for this system at equilibrium potential. (C) Nyquist plot with simulation model data (line) and experimental data (dots) for 1 and 10 $\mu$M dimethylamino-methyl-ferrocene.

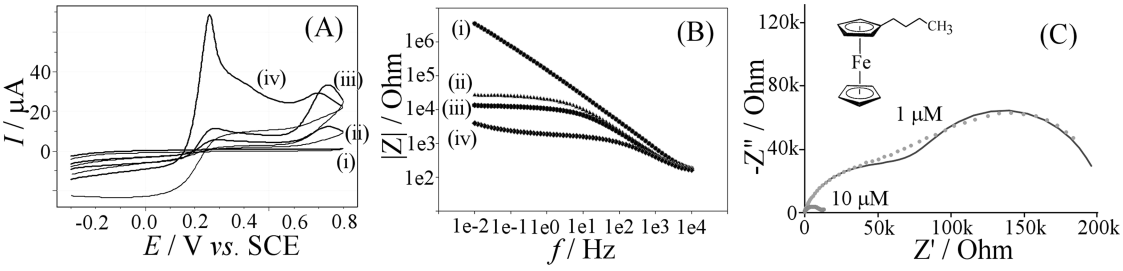


**Figure 9.** (A) Cyclic voltammograms (scan rate = 50 mV $s^{-1}$) for a 3 mm glassy-carbon electrode immersed in aqueous 5 mM $Fe(CN)_6^{3-}$, 5 mM $Fe(CN)_6^{4-}$, and 0.1 M $KNO_3$ with addition of (i) 0, (ii) 5, (iii) 10, and (iv) 50 $\mu$M butyl ferrocene. (B) Impedance data for this system at equilibrium potential. (C) Nyquist plot with simulation model data (line) and experimental data (dots) for 1 and 10 $\mu$M butyl ferrocene.



DOI: 10.1021/acsami.5b03654
ACS Appl. Mater. Interfaces 2015, 7, 15458−15465

additional electrostatic repulsion (at neutral pH) of the negatively charged ferrocene-acetate and the $Fe(CN)_6^{3-/4-}$ redox system is likely to limit further the electron shuttle efficiency. The impedance at the equilibrium potential shows very similar features compared to the data for ferrocene-acetonitrile, with somewhat lower impedance for higher ferrocene mediator concentration.

The (dimethylaminomethyl)ferrocene electron shuttle (Figure 8) is positively charged in neutral aqueous solution with possible implication on reactivity. Voltammetric responses shown in in Figure 8A are consistent with redox mediator activity but with an additional shift in the response and a high peak current at 50 $\mu$M (dimethylaminomethyl)ferrocene concentration. Voltammetric data in Table 2 suggest that (dimethylaminomethyl)ferrocene should be similar in reactivity when compared to ferrocene dimethanol; therefore, the additional anodic current (and the unusually sharp peak shape) may be associated with additional complexity, e.g., favorable interaction with the modified surface or between cationic (dimethylaminomethyl)ferrocene and $Fe(CN)_6^{3-/4-}$ at the electrode surface.

Finally, butyl ferrocene is employed as electron shuttle (Figure 9), and similar trends are observed. The solubility of butyl ferrocene in the aqueous phase is low, and at 50 $\mu$M nominal concentration, additional anodic activity is clearly seen in Figure 9A (a sharp peak), caused by aggregation at the electrode surface. It is likely that at lower butyl ferrocene concentration accumulation of the more lipophilic redox probe into the KolliphorEL film occurs to further aid the electron shuttle process.

On the basis of the qualitative comparison of electron shuttle efficiency, it appears likely that improved mediator effects are linked to (i) ferrocene derivatives with higher rate of electron transfer across the KolliphorEL layer and (ii) ferrocene derivatives with the ability to bind or aggregate at the KolliphorEL surface. A more detailed investigation of the underlying mechanism is presented next.

**3.3. KolliphorEL Grafting Affecting Heterogeneous Electron-Transfer Kinetics: Mechanism.** The equivalent circuit describing the electron shuttle mechanism reasonably closely is shown in Figure 10. The solution resistance $R_{sol}$ and

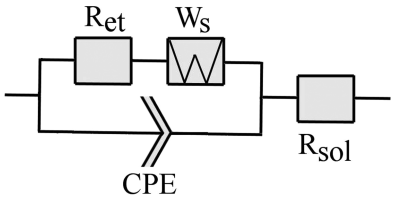


**Figure 10.** Schematic drawing of the equivalent circuit associated with the modified electrode in contact to the solution.

the resistance for heterogeneous electron transfer to the ferrocene derivative $R_{et}$ are complemented with a "short" Warburg impedance to represent, at least at first approximation, the $Fe(CN)_6^{3-/4-}$ redox system feeding electrons into the layer, and a constant phase element (CPE) is employed to cope with nonideal capacitive behavior (caused by pores and heterogeneity at the surface). The short Warburg impedance is acceptable as a description of the mechanism here as long as the concentration of $Fe(CN)_6^{3-/4-}$ is not perturbed, thereby resulting in additional diffusion contributions. This condition is valid only for low ferrocene concentrations, and it seems to give reliable results only for (dimethylaminomethyl)ferrocene and butyl ferrocene (vide infra).

Data summarized in Table 2 describe the results from quantitative impedance data fitting (Figures 5C–9C). It can be observed that the $R_{sol}$ value changes insignificantly, and capacitance $C$ also remains similar to the value observed for the bare glassy-carbon electrode. $R_{et}$ appears to be in the kilo-ohm range, without a clear trend attributable to the structure of ferrocene derivatives. An interesting parameter is $W_T$, which for the short Warburg element, is linked to the apparent diffusion layer thickness $\delta_{app} = (W_T \times D)^{1/2}$ (with $D = 0.6 \times 10^{-9}$ m$^2$ s$^{-1}$ here estimated for the ferrocene derivatives[20]). When inspecting the apparent diffusion layer thickness $\delta_{app}$, it is obvious that all values from 41 to 486 $\mu$m are considerably greater than the thickness of the KolliphorEL film grafted onto the electrode. Therefore, diffusion of ferrocene and ferricenium may occur well within the solution phase (Figure 2). Some of the $\delta_{app}$ values are considerable, which suggests that another type of physical process (such as slow bimolecular electron transfer or an additional heterogeneous electron transfer) could be hidden within the data. It is also interesting that although the first three ferrocene derivatives show a decrease in $\delta_{app}$ with higher mediator concentration (dimethylaminomethyl)-ferrocene and butyl ferrocene show an increase in $\delta_{app}$ with ferrocene concentration. The increase is expected when considering a stronger perturbation of the $Fe(CN)_6^{3-/4-}$ concentration; however, the decrease again suggests another type of physical process underlying the overall process. These trends are also observed in the corresponding data for 5 and 50 $\mu$M ferrocene mediator (not shown).

For the three more-soluble ferrocenes (ferrocene dimethanol > ferroceneacetonitrile > ferroceneacetic acid), a clear trend of lower $\delta_{app}$ for more efficient electron shuttling is seen (see for comparison voltammetry data). The most effective electron shuttle here appears to be (dimethylaminomethyl)ferrocene with the smallest diffusion length $\delta$ = 41 $\mu$m at 1 $\mu$M concentration. It is likely that this is linked to some binding of the electron shuttle to the KolliphorEL film and an indication that in future for this type of ferrocene even lower mediator concentrations are effective.

Finally, the effect of the $Fe(CN)_6^{3-/4-}$ redox system in the aqueous phase is assessed. Figure 11A shows data for a KolliphorEL-modified electrode immersed in solutions of 5, 10, 20, and 50 mM each of $Fe(CN)_6^{3-}$ and $Fe(CN)_6^{4-}$. The increase in the rate of electron transfer provides evidence for the first-order nature of the heterogeneous electron transfer. Impedance data in Figure 11B further demonstrate this effect. Finally, in the presence of 50 $\mu$M butyl ferrocene electron shuttle, an increase in the current response and change in peak shape are seen (Figure 11C), consistent with the voltammetric responses at high mediator concentration being (i) first-order in $Fe(CN)_6^{3-/4-}$ and (ii) now in part $Fe(CN)_6^{3-/4-}$ diffusion-controlled.

## 4. CONCLUSIONS

KolliphorEL has been shown to form monolayer films on glassy carbon when an anodic grafting protocol is applied. Given the ability of KolliphorEL to carry guest species, it is shown here for the first time that guest ferrocene derivatives can be employed to transport electrons across the KolliphorEL monolayer. For a range of ferrocene electron shuttle systems, a comparison and kinetics analysis were conducted and shuttle efficiencies evaluated. For all systems, the anodic process


DOI: 10.1021/acsami.5b03654
ACS Appl. Mater. Interfaces 2015, 7, 15458–15465

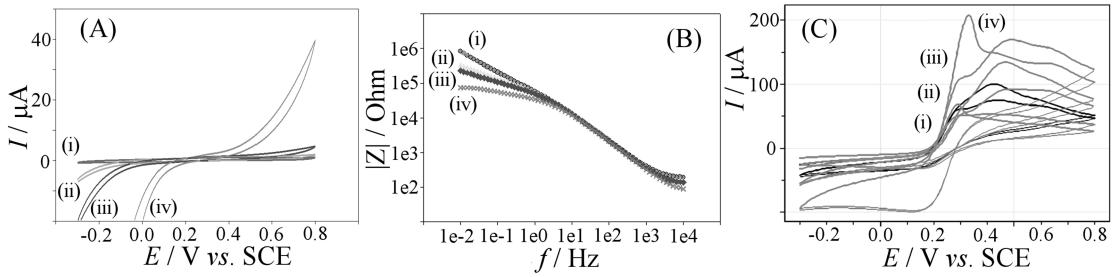


**Figure 11.** (A) Cyclic voltammograms (scan rate = 50 mV $s^{-1}$) for a 3 mm glassy-carbon electrode immersed in aqueous (i) 5, (ii) 10, (iii) 20, and (iv) 50 mM $Fe(CN)_6^{3-}$ and $Fe(CN)_6^{4-}$ in 0.1 M $KNO_3$. (B) Impedance data for the same system at equilibrium potential. (C) Cyclic voltammograms in the presence of 50 $\mu$M butyl ferrocene and with varying $Fe(CN)_6^{3-/4-}$ concentration.

appears to be considerably faster compared to the cathodic process (causing apparent irreversibility), in line with ferrocenes generally being oxidized at more positive potentials compared to $Fe(CN)_6^{3-/4-}$. The key parameters affecting the electron shuttle effect are (i) binding or aggregation ability predominantly on the basis of hydrophobicity and (ii) ability to penetrate the KolliphorEL film with faster heterogeneous electron transfer. At low concentration especially, butylferrocene and (dimethylaminomethyl)ferrocene are highly effective.

In future, a wider range of electron shuttle systems could be evaluated in particular with the aim of detecting very low concentrations of redox-active molecules (drugs, biomarkers, pollutants, etc.). It will be interesting to explore lower concentrations and more hydrophobic mediator systems.

## AUTHOR INFORMATION

### Corresponding Author

*E-mail: f.marken@bath.ac.uk.

### Notes

The authors declare no competing financial interest.

## ACKNOWLEDGMENTS

C.E.H. thanks the University of Bath for a Ph.D. scholarship. K.N. thanks LUT for financial support.

## REFERENCES

(1) Mandler, D.; Kraus-Ophir, S. Self-assembled Monolayers (SAMs) for Electrochemical Sensing. *J. Solid State Electrochem.* **2011**, *15* (7–8), 1535–1558.

(2) Liu, J. Q.; Liu, Z.; Barrow, C. J.; Yang, W. R. Molecularly Engineered Graphene Surfaces for Sensing Applications: A review. *Anal. Chim. Acta* **2015**, *859*, 1–19.

(3) Ates, M.; Sarac, A. S. Conducting Polymer Coated Carbon Surfaces and Biosensor Applications. *Prog. Org. Coat.* **2009**, *66* (4), 337–358.

(4) Murray, R. W. Chemically Modified Electrodes. *Acc. Chem. Res.* **1980**, *13* (5), 135–141.

(5) Gooding, J. J. Advances in Interfacial Design Sensors: Aryl Diazonium Salts for Electrochemical Biosensors and for Modifying Carbon and Metal Electrodes. *Electroanalysis* **2008**, *20* (6), 573–582.

(6) Allongue, P.; Delamar, M.; Desbat, B.; Fagebaume, O.; Hitmi, R.; Pinson, J.; Saveant, J. M. Covalent Modification of Carbon Surfaces by Aryl Radicals Generated from the Electrochemical Reduction of Diazonium Salts. *J. Am. Chem. Soc.* **1997**, *119* (1), 201–207.

(7) Decreau, R. A.; Collman, J. P.; Hosseini, A. Electrochemical Applications. How Click Chemistry Brought Biomimetic Models to the Next Level: Electrocatalysis under Controlled Rate of Electron Transfer. *Chem. Soc. Rev.* **2010**, *39* (4), 1291–1301.

(8) Abiman, P.; Wildgoose, G. G.; Crossley, A.; Jones, J. H.; Compton, R. G. Contrasting pKa of Protonated Bis(3-aminopropyl)-terminated Polyethylene Glycol "Jeffamine" and the Associated Thermodynamic Parameters in Solution and Covalently Attached to Graphite Surfaces. *Chem. - Eur. J.* **2007**, *13* (34), 9663–9667.

(9) Chow, E.; Gooding, J. J. Peptide Modified Electrodes as Electrochemical Metal Ion Sensors. *Electroanalysis* **2006**, *18* (15), 1437–1448.

(10) Belanger, D.; Pinson, J. Electrografting: a Powerful Method for Surface Modification. *Chem. Soc. Rev.* **2011**, *40* (7), 3995–4048.

(11) Maeda, H.; Saka-iri, Y.; Ogasawara, T.; Huang, C. Z.; Yamauchi, Y.; Ohmori, H. Anodization in Oligo(ethylene glycol) as an Initial Derivatization Tool for Preparing glassy-carbon electrodes Covalently Modified with Amino Compounds: Effective Access to a 2,2,6,6-Tetramethylpiperidinyl-1- oxyl (TEMPO)-Modified glassy-carbon electrode. *Chem. Pharm. Bull.* **2001**, *49* (10), 1349–1351.

(12) Maeda, H.; Itami, M.; Katayama, K.; Yamauchi, Y.; Ohmori, H. Anodization of glassy-carbon electrodes in Oligomers of Ethylene Glycol And their Monomethyl Ethers as a Tool for the Elimination of Protein Adsorption. *Anal. Sci.* **1997**, *13* (5), 721–727.

(13) Maeda, H.; Kitano, T.; Huang, C. Z.; Katayama, K.; Yamauchi, Y.; Ohmori, H. Effective Method for the Covalent Introduction of the 2-(2- Carboxymethoxyethoxy)ethoxy Group on a glassy-carbon electrode by Anodization in Triethylene Glycol. *Anal. Sci.* **1999**, *15* (6), 531–536.

(14) Hotchen, C. E.; Maybury, I. J.; Nelson, G. W.; Foord, J. S.; Holdway, P.; Marken, F. Amplified Electron Transfer at Poly-Ethylene-Glycol (PEG) Grafted Electrodes. *Phys. Chem. Chem. Phys.* **2015**, *17*, 11260–11268.

(15) Maeda, H.; Yamauchi, Y.; Hosoe, M.; Li, T. X.; Yamaguchi, E.; Kasamatsu, M.; Ohmori, H. Direct Covalent Modification of Glassy Carbon Surfaces with 1-Alkanols by Electrochemical Oxidation. *Chem. Pharm. Bull.* **1994**, *42* (9), 1870–1873.

(16) Gelderblom, H.; Verweij, J.; Nooter, K.; Sparreboom, A. Chremophor EL: the Drawbacks and Advantages of Vehicle Selection for Drug Formulation. *Eur. J. Cancer* **2001**, *37* (13), 1590–1598.

(17) Ishihara, H. Current Status and Prospects of Polyethyleneglycol-Modified Medicines. *Biol. Pharm. Bull.* **2013**, *36* (6), 883–888.

(18) Barnes, E. O.; Lewis, G. E. M.; Dale, S. E. C.; Marken, F.; Compton, R. G. Generator-Collector Double Electrode Systems: A review. *Analyst* **2012**, *137* (5), 1068–1081.

(19) Wang, X. Y.; Pang, G. C. Amplification Systems of Weak Interaction Biosensors: Applications and Prospects. *Sens. Rev.* **2015**, *35* (1), 30–42.

(20) Si, Y. M.; Sun, Z. Z.; Zhang, N.; Qi, W.; Li, S. Y.; Chen, L. J.; Wang, H. Ultrasensitive Electroanalysis of Low-Level Free microRNAs in Blood by Maximum Signal Amplification of Catalytic Silver Deposition using Alkaline Phosphatase-Incorporated Gold Nanoclusters. *Anal. Chem.* **2014**, *86* (20), 10406–10414.

(21) (a) Wagner, C. D.; Davis, L. E.; Zeller, M. V.; Taylor, J. A.; Raymond, R. M.; Gale, L. H. *Surf. Interface Anal.* **1981**, *3*, 211. (b) Wagner, C. D. Appendix 6. In *Practical Surface Analysis*, 2nd ed.; Briggs, D., Seah, M. P., Eds.; J. Wiley and Sons: New York, 1990; Vol. *1*.

(22) Ferro, S.; Dal Colle, M.; De Battisti, A. Chemical Surface Characterization of Electrochemically and Thermally Oxidized Boron-Doped Diamond Film Electrodes. *Carbon* **2005**, *43* (6), 1191–1203.



DOI: 10.1021/acsami.5b03654
ACS Appl. Mater. Interfaces 2015, 7, 15458–15465

(23) Schlapak, R.; Caruana, D.; Armitage, D.; Howorka, S. Semipermeable Poly(ethyleneglycol) Films: the Relationship Between Permeability and Molecular Structure of Polymer Chains. *Soft Matter* **2009**, *5*, 4104−4112.
(24) Xiong, L. H. J.; Batchelor-McAuley, C.; Ward, K. R.; Downing, C.; Hartshorne, R. S.; Lawrence, N. S.; Compton, R. G. Voltammetry at Graphite Electrodes: The Oxidation of Hexacyanoferrate (II) (Ferrocyanide) does not Exhibit Pure Outer-Sphere Electron Transfer Kinetics and is Sensitive to Pre- Exposure of the Electrode to Organic Solvents. *J. Electroanal. Chem.* **2011**, *661* (1), 144−149.
(25) French, R. W.; Collins, A. M.; Marken, F. Growth and Application of Paired Gold Electrode Junctions: Evidence for Nitrosonium Phosphate During Nitric Oxide Oxidation. *Electroanalysis* **2008**, *20* (22), 2403−2409.


DOI: 10.1021/acsami.5b03654
*ACS Appl. Mater. Interfaces* 2015, 7, 15458−15465